Efficient Ray-Tracing Techniques for Three-Dimensional Analyses of Propagation in Mobile Communications: Application to Picocell and Microcell Scenarios

M. F. Cátedra, J. Pérez, F. Saez de Adana, and O. Gutierrez

Grupo de Sistemas y Radio
Dpto de Ingeniería de Comunicaciones
Universidad de Cantabria
39005 Santander
Spain
Tel: + 34 42 201493
Fax: + 34 42 201873
E-mail: felipe@gsr.unican.es

Keywords: Geometrical Theory of Diffraction; Uniform Theory of Diffraction; land mobile radio cellular systems; land mobile radio propagation factors

1. Abstract

The application of several ray-tracing techniques, in combination with GTD/UTD (Geometrical Theory of Diffraction/Uniform Theory of Diffraction), for an efficient analysis of propagation in urban scenarios is presented. The frequency of the analysis is in the UHF band, and a three-dimensional model of the geometry, using flat facets, is considered. After a review of the most commonly used ray-tracing techniques, a new method, called the Angular Z-Buffer (AZB) technique, is presented. As is shown and validated with results, the AZB appears to be extremely efficient for GTD/UTD applications.

2. Introduction

Traditionally, empirical methods [1] have been preferred for mobile communications, for both rural and urban cells. In these methods, the specific data of each scenario are considered only in a statistical sense (e.g., the average height of buildings, the average width of streets, etc.). It is assumed that the transmitting antenna is in a predominant location in the cell (a high tower, hill, etc.), and that the receiver is shadowed by a relatively large number of obstacles, such as buildings, hills, etc. In these situations, the empirical models give reasonably good predictions.

However, when increasing traffic requires a mobile architecture with quite small microcells or "picocells," and when the transmitting antenna is in a moderately low position, the statistical assumptions of the empirical methods do not work any more. This is because we do not have a large number of obstacles shadowing the receiver. In these cases, the propagation parameters in the cell will be obtained by on-site measurements, or by deterministic computations considering a realistic geometrical and physical model of the particular scene to be analyzed. If the computer tools, based on the deterministic models, are efficient and reliable, they are preferable to measurement campaigns.

Propagation tools require site-specific information for the particular environment. In urban microcellular scenarios, the received signal is composed of energy reflected, transmitted, or diffracted by buildings. Additional signals, scattered from trees, lamps, telephone boxes, etc., can be neglected [2]. Therefore, data required for the propagation models consist of the geometrical and electrical characteristics of buildings in the microcell. Buildings and terrain are modeled geometrically by means of polygonal plane facets (infinitely thin). Inside buildings, walls and floors are represented as polygonal plane facets, as well. As in urban environments, additional small obstacles, such as furniture, are not taken into account in propagation models. Therefore, in both cases, the propagation tools work in a three-dimensional world of polygonal flat facets that model the obstacles of the scene.

The field strength at the receiver is obtained as the sum of the fields associated with the rays that connect the transmitting antenna with the receiver. A completely three-dimensional GTD/UTD electromagnetic model is considered. Rays can suffer reflections on the facets, diffraction on the wedges, and transmission across the facets. Antennas are assumed to be infinitely small.

Mainly, two strategies have been proposed in the propagation models: the "pincushion" method [2-4], and the multiple-image method [5-7]. The primary function of the ray-tracing tool is to determine if a ray hits a facet. As the number of facets increases linearly, the number of intersection tests increases exponentially. Thus, in high-complexity environments, such as urban and indoor scenarios, all propagation models require ray-tracing acceleration techniques, in order to reduce CPU times and memory requirements. The reduction is achieved by minimizing the number of times that the rigorous algorithms are applied.

This paper addresses the rationale for using ray-tracing techniques, as presented in Section 3. A comparison between the needs for visualization applications and for radiowave propagation in the UHF band is presented in Section 4. Computer visualization of complex scenes has received a great interest in the last 30 years in many areas: flight simulators, computer movies, virtual reality, scientific visualization, etc. Therefore, a large amount of effort has been expended to develop ray-tracing tools for computer visualiza-

 1045-9243/98/$10.00©1998 IEEE

tion. The diffraction phenomena are not important in computer visualization, where the aim is to represent the scenes as they are seen by the human eye (of course, this is only sensible in the "visible" part of the electromagnetic spectrum). However, diffraction in the UHF band is key to explaining the field coverage in the shadowed areas of the cell. This means that none of the ray-tracing algorithms for visualization can be directly applied to the UHF problem. A survey of the most commonly used ray-tracing techniques for the UHF band is presented in Section 5, together with a classification of these in terms of direct and inverse algorithms. The direct algorithms, such as the pincushion or shooting-and-bouncing-ray algorithms, are not very well suited to treat diffraction, as shown in Section 5. Inverse algorithms do not have this limitation, and therefore they are more appropriate to treat the UHF-propagation problem.

Among the inverse methods are the Binary Space Partitioning (BSP) method, the Space Volumetric Partitioning (SVP) method, and the Angular Z-Buffer (AZB) method. The application of the BSP method will be described in a companion paper. The SVP method, also known as the "Bounding Volumes" method, is presented and compared with the AZB technique. The AZB technique has been developed by the authors of this paper, and is quite efficient when a large number of observation points is illuminated by the source or by any equivalent source (images of reflections, diffraction edges, etc.).

A computer tool, called *FASPRO*, based on a three-dimensional GTD/UTD formulation and on the AZB technique, has been developed to check the accuracy of the formulation and the efficiency of the ray-tracing technique. Comparisons with measurements considering simple and double coupling mechanisms (direct, reflected, diffracted, double-reflected, diffracted-reflected, reflected-diffracted, etc.) show that the model is reliable enough: at least, better than methods based on the use of reflections of very high order [7]. Considering that *FASPRO* only requires a CPU time of a few minutes with a Pentium machine for the analysis of a complex urban scene, using a fine mesh of observation points (e.g., 10,000 points), it can be said that the AZB ray-tracing algorithm is quite efficient for design purposes in mobile-communication applications.

3. Rationale for ray tracing

In a complex urban scene, such as shown in Figure 1, we can have a large number of buildings, N_b, each one of them with its own height and characteristic material. To simplify, we will assume that all the buildings are defined by flat polygonal facets, and that each building is defined by some vertical facets and one horizontal facet, to represent the roof top. In this way, an ensemble of N_v vertical facets, N_h horizontal facets, M_v vertical edges, and M_h horizontal edges describes the scene. We must accept that each one of these numbers can be of the order of hundreds.

In a mobile-communication problem, we will have to compute the field at points located in the nodes of a mesh or, in some cases, along a path. The source can be located at any arbitrary point in the scene. Usually, the number of observation points, N_0, is quite large, probably of the order of thousands or even greater. In these cases, most of the CPU time (90% or more) can be consumed in the following geometrical testing:

• Test if the ray path between an observation point is shadowed by at least one facet of the scene.

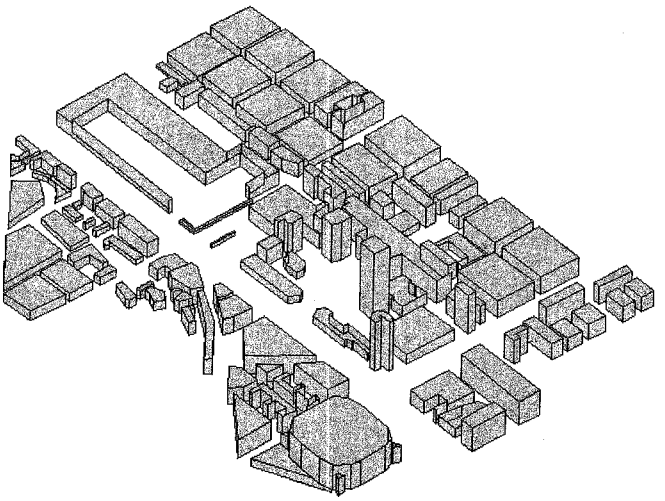

Figure 1. A three-dimensional view of an urban scene.

• Determine which facets or edges can participate in a coupling mechanism (e.g. reflection, diffraction, double reflection, etc.)

The most-naive procedure for performing this testing is to consider all the facets of the scene, one by one. If N and M are the total numbers of facets and edges, this means performing shadowing testing a number of times proportional to

$N_0(N+M)N$ for first-order effects (the direct ray and the simple reflected and diffracted rays);

$N_0(N+M)^2N$ for second-order effects (double-reflected rays, diffracted-reflected rays, etc.);

$N_0(N+M)^3N$ for third-order effects (triple-reflected rays, diffracted-double-reflected rays, etc.);

and so on.

For the first-order effect, the number can be typically of the order of billions, while for the second-order case, we can easily have trillions. For third- or higher-order cases, the number can become incomprehensible. Therefore, the need to avoid this tremendously large amount of shadowing tests appears evident. To do this, we must use efficient ray-tracing techniques. It must be noted that the shadowing test requires the computation of several products and sums that should be avoided, if possible.

4. Ray-tracing techniques for visualization and for UHF propagation

Most of the ray-tracing techniques have been developed in the last three decades for computer-visualization applications [8-9]. A source of light of incoherent nature is assumed for the scene illumination in these applications. Comparing these applications with an urban-propagation problem at a frequency of about 900 MHz, we found several common aspects, but also some important differences. These are mainly as follows:

• In the UHF case, the source is coherent, and phase and polarization are important.

• Edge-diffraction plays an important role in the UHF case. Deeply shadowed areas can be reached, thanks to the diffraction-field coverage.

• Reflections in the light-illumination problem are nearly always diffuse, while in the UHF band, they are predominantly specular.

Of course, when the frequency increases, the differences between radio propagation and the visualization problem decrease.

To deal with these differences, some important cautions should be taken (e.g., special care with the coordinate-system transformations, with the polarization calculations, diffraction coupling, etc.). Therefore, no ray-tracing technique for visual applications can be applied directly to the UHF problem.

In order to illustrate the importance of diffraction in UHF, simulations with and without diffracted rays have been considered for the urban scene of Figure 1. In particular, the following cases are presented here:

- Case 1: only direct and reflected rays, in Figure 2;
- Case 2: direct, reflected and diffracted rays, in Figure 3;
- Case 3: all the rays of Figure 3, plus double-reflected rays, diffracted-reflected rays, and reflected-diffracted rays, in Figure 4.

Examining Figures 2-4, we can conclude that wide coverage is achieved by the diffraction mechanism, which becomes the primary factor in areas in the shadow of the direct or reflected rays. In some works [2-4], the coverage in these shadowed areas is computed considering reflections of very high order. However, as we will see in the results section, these approaches do not always accurately follow the measurements.

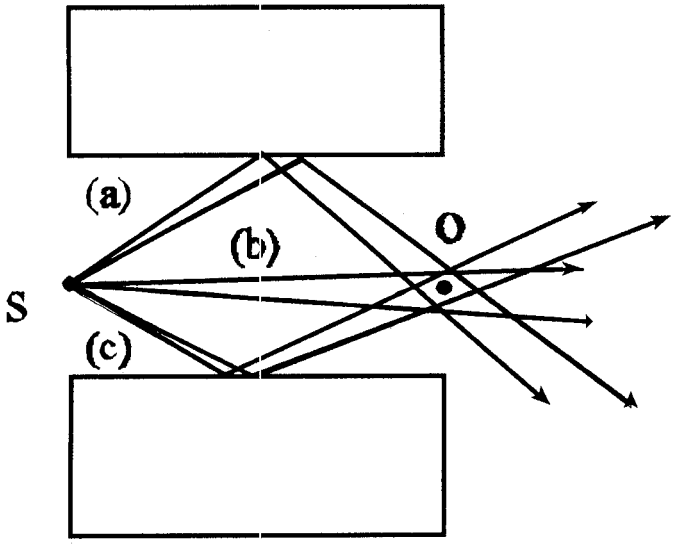

Figure 5. Using a direct algorithm, ray tubes are launched from the source in all directions, covering the complete angular space seen from the source (4π steradians). Three tubes are shown as reaching the observation point, O.

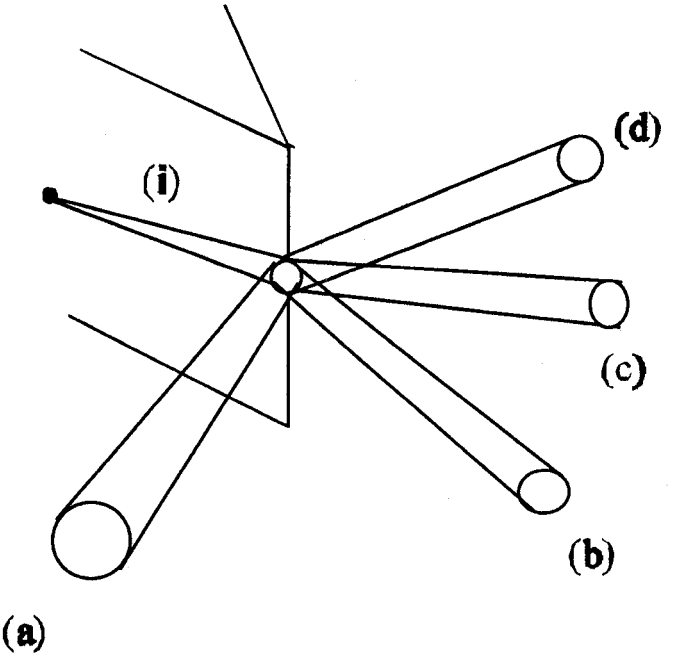

Figure 6. An incident tube of rays (i) originates a large number of new ray tubes when it hits an edge. All the new tubes are around the Keller cone. Four of these tubes, (a), (b), (c), and (d), are pictured.

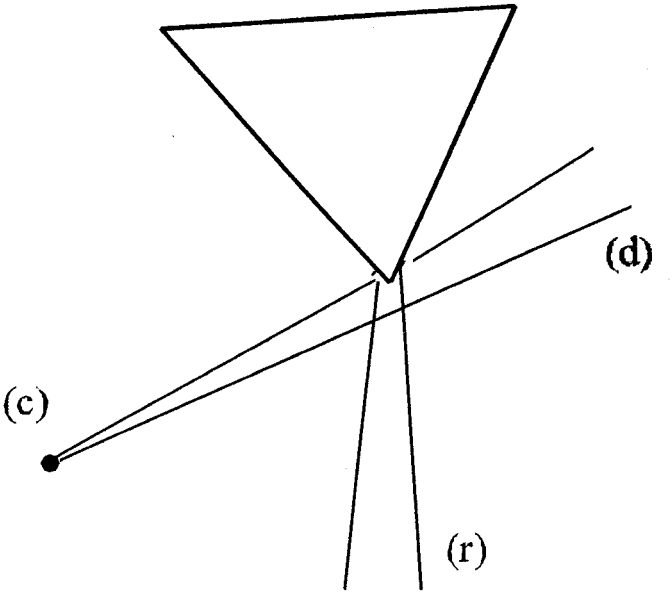

Figure 7. A perpendicular cut of a diffraction problem: (c) is the incident ray tube; (d) is the diffracted tube located in the lit boundary; and (r) is the diffracted tube located in the reflection boundary.

5. Survey of ray-tracing algorithms

We can classify the ray-tracing techniques into two groups.

5.1 Direct Algorithms

Direct algorithms (pincushion, shooting-and-bouncing rays, etc.) are those in which the ray tubes are shot from the source to all of the space directions [2-4]. The trajectory of each tube of rays is

analyzed by allowing the tube to propagate in the space, following all its impacts with the facets, as shown in Figure 5. Usually, when the tube advances, its cross section increases. When the tube reaches the observation point, the previously computed field-intensity level at the point is annotated with the tube contribution to the field level. The observation point is usually reached by lots of tubes. It must be noted that the evaluation of the field at the observation point is not complete until its corresponding tube has covered all the space seen from the source.

Direct algorithms have been widely used in urban scenes, even for the UHF band. In general, they work well for visualization problems. However, they present serious difficulties in the UHF band. One problem is that when a tube of rays reaches the edge of a wedge, it suffers diffraction, as is shown in Figure 6. This creates a catastrophe for the tube, because the area of the wedge where the incident tube impacts behaves as a new source of ray tubes, located around the Keller cone, as can be seen in Figure 6. Also, the computation of the field transported by each one of the ray tubes generated in the diffraction is very cumbersome, because the diffracted field is not a spherical wave, as is usually assumed in most pincushion algorithms. The difficulties of computation increases when we consider the diffracted tubes of rays, located in the lit boundary and reflection boundaries, as shown in Figure 7.

Another difficulty of the direct algorithms appears when the phase of the field must be computed. It is true that the density of power per square meter and, therefore, the field magnitude, can be found easily, considering the spreading of the cross section of the tube, and applying the law of energy conservation. However, the phase can not be found with enough accuracy from the knowledge of the tube cross section. This is especially true when the stigmatic tube is not spherical (for instance, after diffraction), because in this case, it is quite difficult to find which is the wave front of the observation point. The phase of the field at this observation point is obtained from the distance of this wavefront to the wave-reference surface.

5.2 Inverse algorithms

Using these algorithms, an inverse problem is solved: given the geometry of the scenario, the source and the observation points, we find all the ray paths (direct, reflected, diffracted, etc.) that connect both points [5-6]. For instance, for the reflected ray, we must check

1. All the facets which are visible for both the source and observations points.

2. For each one of the visible facets, we must test to see if there is a reflection that follows Snell's laws, has the reflection point within the polygon of the facet, and with the paths SR and RO not shadowed by any other facet.

An inverse algorithm is, in general, more complicated that a direct algorithm, because we must check all possible paths connecting S and O. However, inverse algorithms are well suited to accurately compute diffraction, phase, and polarization. These aspects, as we mentioned above, can be essential for an urban-propagation problem in the UHF band. For these reasons, we have selected the inverse method for the UHF-band propagation analysis.

In any case, the direct and inverse methods have some ray-tracing steps in common: the testing for shadowing by the facets of a line connecting a pair of points. An inverse algorithm also requires an efficient way to discard facets, edges, etc., that do not contribute to reflections, diffraction, etc.

5.3 Space Volumetric Partitioning (SVP)

One of the earlier techniques utilized to reduce the number of facets to be checked in the shadowing analysis of a path is the SVP technique, also known as the "Bounding Volumes" algorithm [8-9]. Using SVP, the space is divided into a set of N_x elemental cells, as shown in Figure 8. These cells are the elemental volumes of the technique, and following the specialized literature, they can be called *voxels* (elemental volumes), in analogy to *pixels*, a commonly used abbreviation of "picture elements" [10].

It is assumed that each facet of the scene can be identified by a facet number, `FN`. From the `FN` of a facet we can find the geometrical parameters that characterize the facet in the matrix `FACET(N,L)`. For instance, the facet with `FN = j` has all its geometrical data in the column `FACET(j,k), k = 1,2,L`.

A column of a matrix called `SVP` is assigned to each voxel. For instance, the column `(i)`, defined as `SVP(i,j), j = 1,2,Nf`, is assigned to the voxel number `(i)`. If `Ni` is the actual number of facets in voxel `(i)`, then the first `Ni` terms of column `(i)` contain the `FN` of the facets of the voxel. The other `Nf-Ni` terms of the column are made equal to zero. Figure 9 can be used to outline the way in which the SVP works. If we consider the path SO of the figure, it is evident that we must start the checking to detect the path shadowing either by the facets located in the voxel

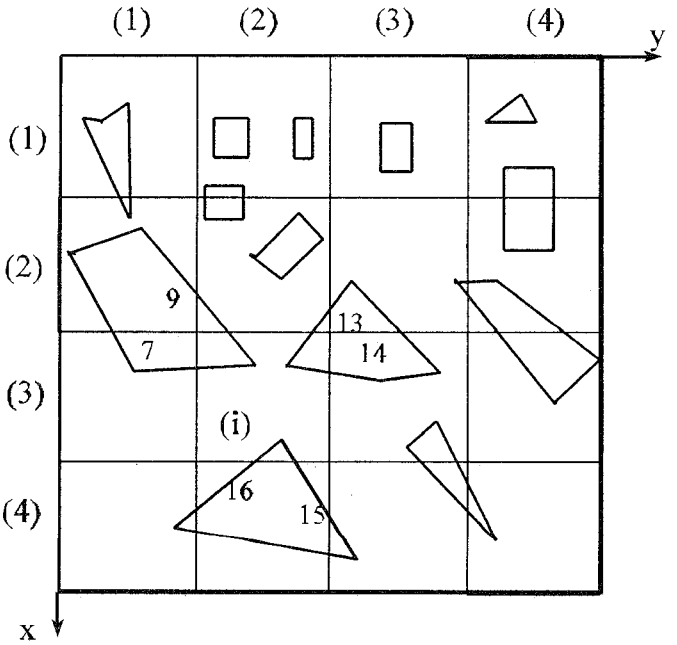

Figure 8. A horizontal cut of an urban scene. Using a regular way of splitting the scene, a set of $N_{xx}N_{yx}N_z$ voxels is obtained (in the figure, $N_x = N_y = 4$, $N_z = 1$). The maximum number of facets per voxel is `Nf`. A facet can belong simultaneously to several voxels. The voxel number (i) has six facets, for which the `FN` are 7, 9, 13, 14, 15, and 16. The first six terms of the column `(i)` of matrix `SVP` are made equal to 7, 9, 13, 14, 15, and 16.

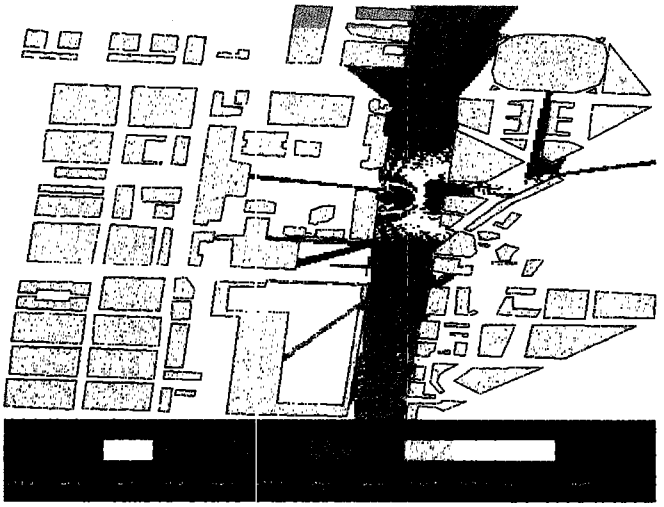

Figure 2. Case 1: The field-coverage level from the direct and the reflected rays for the urban area shown in Figure 1. The solid point indicates the transmitting-antenna location. The frequency is 945.0 MHz.

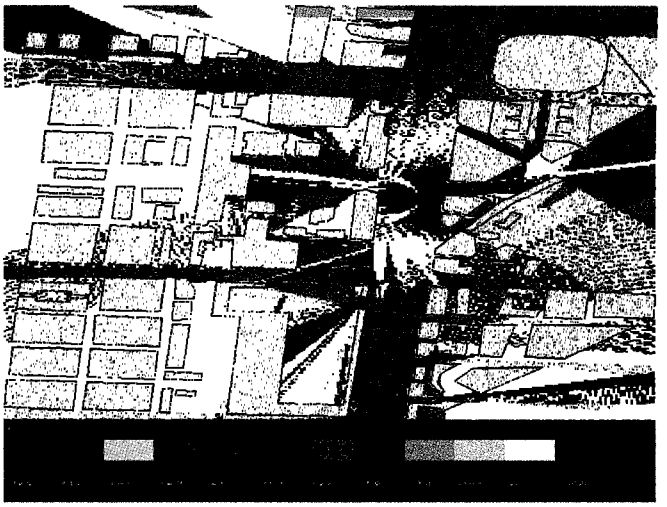

Figure 3. Case 2: The same situation as in Figure 2, but including direct, reflected, and diffracted rays.

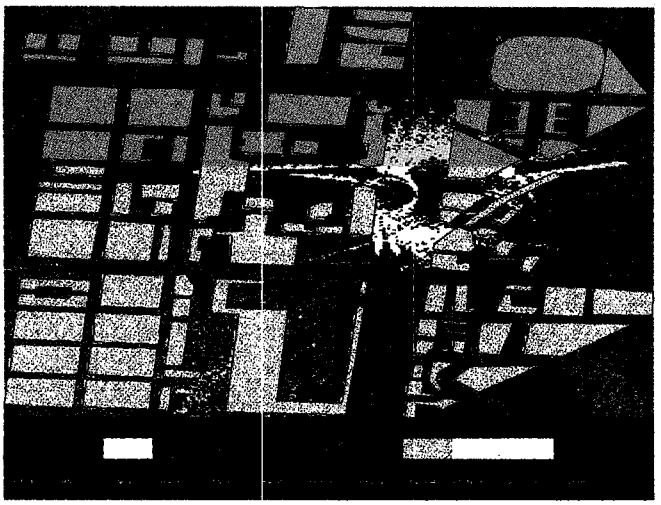

Figure 4. Case 3: The same situation as in Figure 2, but including direct, reflected, and diffracted, double-reflected, diffracted-reflected, and reflected-diffracted rays.

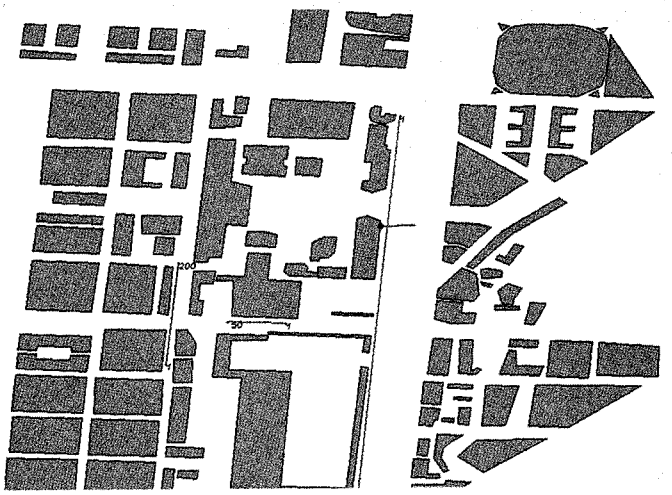

Figure 20. A map of the urban scene shown in Figure 1. The position of the transmitting antenna is indicated by the solid point. The axis of the antenna is represented by a thin line, which extends from the solid point approximately perpendicular to the wall where the antenna has been fixed.

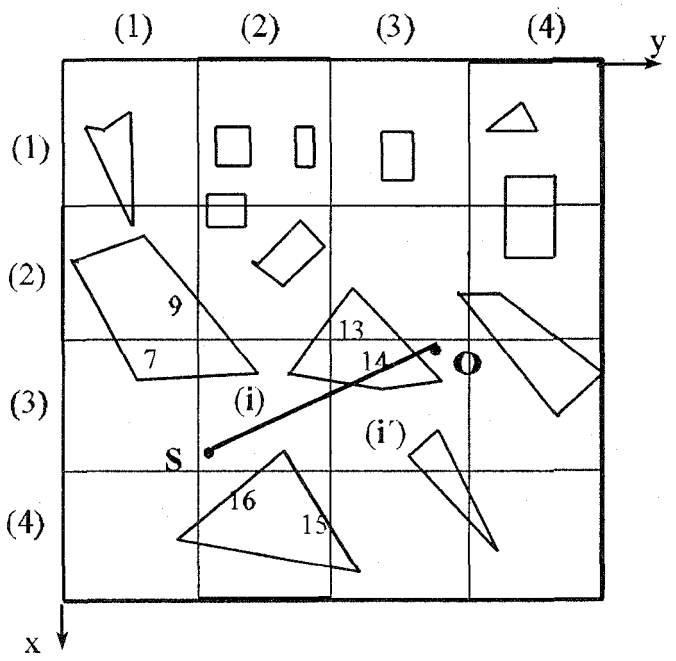

Figure 9. Any possible obstruction of the line SO is investigated only in the voxels crossed by the line. In the case of the figure, this is the situation for voxels (i) and (i').

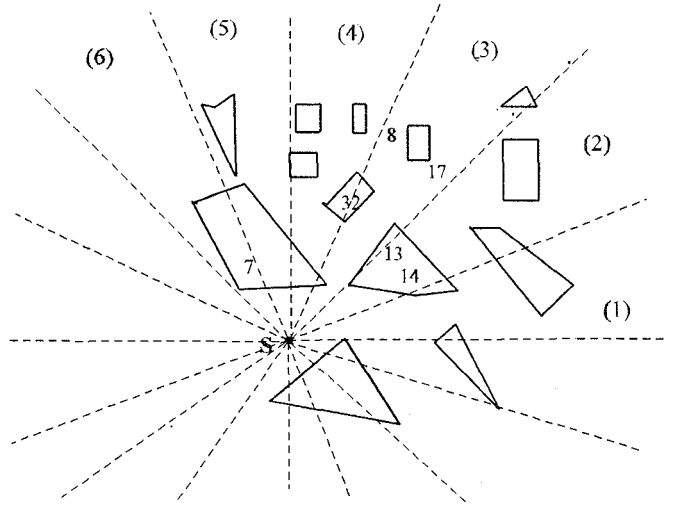

Figure 10. The space is split into angular sectors, "anxels," with a common vertex, the source point S. In the figure, only the first six anxels have been numbered.

(i), where the source S is, or by the voxel (i'), where the observation point O is. Assuming we start with the voxel (i), then we only check the non-null terms of column (i) of matrix SVP, where we can find the FN of all the facets in the voxel. Then, from the FN of these facets, we obtain their geometrical parameters in matrix FACET. Using a rigorous intersection method, we determine if any of these facets shadow the path SO. Doing that, we can note that the number of facets to be checked in voxel (i) of Figure 9 is 6: of course, a number less than N, the total number of facets in the scene. If the shadowing with the facets of the voxel is positive, as is the case in Figure 9, we finish the shadowing test of path SO. If not, we must repeat the process, considering all the voxels that are reached by path SO. We realize that, statistically, the SVP can reduce the shadow-testing time by approximately a factor of Nx, the number of voxels.

The SVP technique can be improved using hierarchically partitioned structures [11], or by using the octree technique [12].

5.4 The Angular Z-Buffer (AZB) technique

The AZB technique, developed by the authors of this paper, resembles, in part, the Light Buffer technique [13]. However, the AZB has a lot of particular features that make it especially well suited for the UHF-propagation problem, and especially for the treatment of diffraction. To describe the AZB algorithm, we will consider separately the cases of direct rays, reflected rays, and diffracted rays.

5.4.1 Direct ray case

We will start the AZB presentation by considering a two-dimensional case. Figure 10 shows the same geometry as for Figures 8 and 9, but now the scene is split into angular sectors, with a common vertex located in the point source S. Using a nomenclature similar to the SVP technique, we will call these angular sectors "*anxels*," as an abbreviation for angular elements.

In the AZB approach, a sub-matrix of a matrix called DAZB is associated with each anxel. The sub-matrix for the anxel (i) is defined by DAZB(i,j,k), j = 1,2,...,Nf; k = 1,2. This sub-matrix can be considered to be formed from a couple of columns, for k = 1 and 2, respectively. The FNs of the facets located in anxel (i) are stored in the column DAZB(i,j,1). At the beginning, the first Ni terms of this column are filled, Ni being the actual number of facets in anxel (i). Until now, the matrix arrangement is similar to the case of the SVP, but now we introduce a very important trick in the way the facets are sorted in the anxel column. They are sorted according to the smallest distance to the source S. We consider that the distance to S of a facet is thus of the closest vertex. Also, and in order to improve the efficiency of the method, once the facets have been sorted, they are checked, starting from the second one, in order to determine if they are shadowed by facets closer to the source. All the facets shadowed are deleted from the column. In this way, at the end of the process we have a number of non-vanishing terms less than (or equal, in the worst case) to the number of facets in the anxel in the column of anxel (i). This procedure of sorting facets in the anxel and

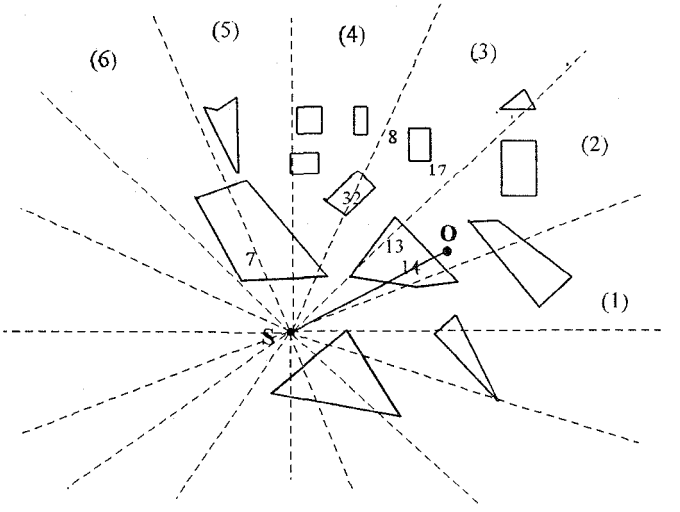

Figure 11. An example of a path to be checked for shadowing.

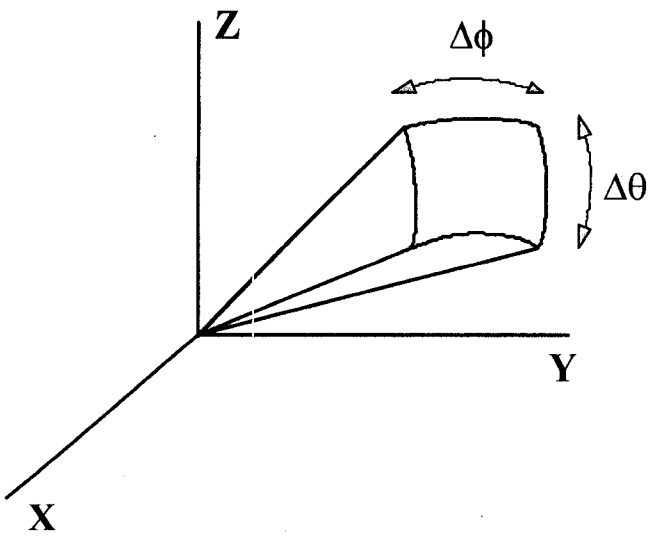

Figure 12. In a three-dimensional problem, the anxel is a small solid-angle increment, $\Delta\theta\Delta\phi$.

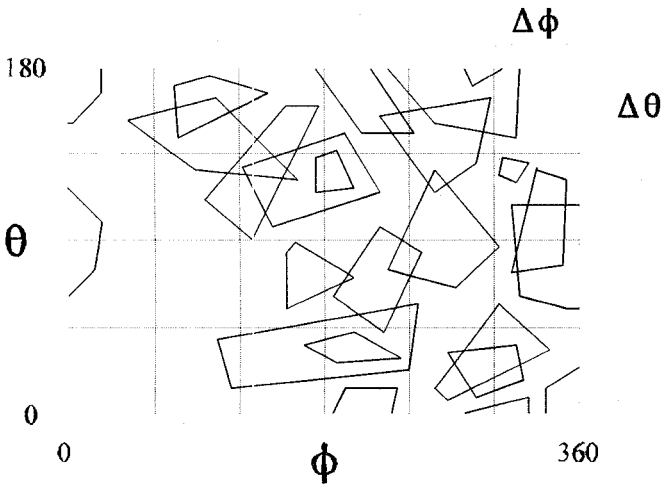

Figure 13. The arrangement of the facets in the anxel meshes, as seen from the source S, and covering the complete angular space.

discarding the shadowed ones is called the "painter's algorithm," [14]. This is because it resembles the way a painter works: nearest objects are painted over the farthest ones, shadowing them. The painter's algorithm is used in most *z*-buffer algorithms. Considering the case of Figure 11, we have only two full terms in column `DAZB(2,j,1)` to store FNs 13 and 14. In the column `DAZB(3,j,1)`, five non-null terms are considered to store FNs: 7, 13, 32, 17 and 8.

Doing the shadow testing of a path SO (see Figure 11), its length is computed and compared with the distance of the facets of the anxel where the path is located. The facet closest to the source is considered first (the first one in the `DAZB` column of FNs of the anxel). If the path length is less than the distance of the closest facet, the path is not shadowed. Elsewhere, a test for shadowing with the closest facet is performed. If the point O is not shadowed, the process is repeated considering the second-closest facet. The shadow testing of SO ends when: a) an obstruction by a closer facet is detected; b) or to the contrary, when the point is not shadowed by the closest facets and is found to be closer than the rest of facets in the anxel. In this last case, the diagnosis is "visible point." The AZB is quite efficient, because for the shadow testing of a point, only some of the closer facets in the anxel are considered.

Until now, the AZB technique has been presented for the two-dimensional case. Its extension for a three-dimensional case is easy: now an anxel is defined as an element of solid angle, as indicated in Figure 12. A grid of anxels, as can be seen in Figure 13, meshes the total angular space seen from the source point, S. The `DAZB` matrix is defined similarly to the two-dimensional case: a sub-matrix `DAZB(i,j,k), j = 1,2...,Nf; k = 1,2,` is associated with the anxel `(i)`. Once the matrix `DAZB` has been defined, the checking for shadowing is similar to the process for the two-dimensional problem, and for brevity it is not repeated here.

Analyzing the advantages of the AZB for the direct ray, we can say that the number of facets to be checked is N_{pa} times less than N_t/N_a, where N_t and N_a are the number of facets in the scene and the number of anxels, respectively. The factor N_{pa} is introduced by the painter's algorithm, and it depends on the anxel mesh. From the authors' experience, it is usual that for a mesh with $\Delta\phi$ less than 2π, the number of facets to be considered in the shadow testing of an observation point is only one or two.

5.4.2 Reflected-ray case

In this case, the sources are the images of the transmitting antenna (S) with respect to the directly illuminated facets. These facets are determined using the `DAZB` matrix of the direct-field computation.

The image points (I) are the sources of the reflected rays. But we must consider that these only radiate in a portion of space (reflection space) determined by the reflecting facet (see Figure 14). The reflection space is seen as a quadrangle in the $\theta_i\phi_i$ space seen from I (θ_i and ϕ_i are the spherical angular coordinates of the axes fixed by the image). The highest and lowest values of θ_i and ϕ_i of this quadrangle determine the angular margins (θ_{max}, θ_{min}, ϕ_{max}, and ϕ_{min}), where the AZB must be applied. We will call the area within these margins the "AZB rectangle" (see Figure 15). As in the direct-field analysis, the AZB rectangle is divided into anxels. Then, for each facet seen from I in its AZB rectangle, the anxel or anxels where it lies are determined to fill the

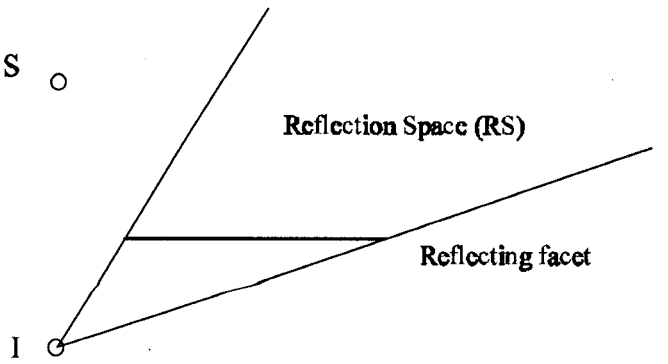

Figure 14. The image I of source S in the facet acts as a new source, but now it radiates only in the space region RS covered by the rays reflected in the facet.

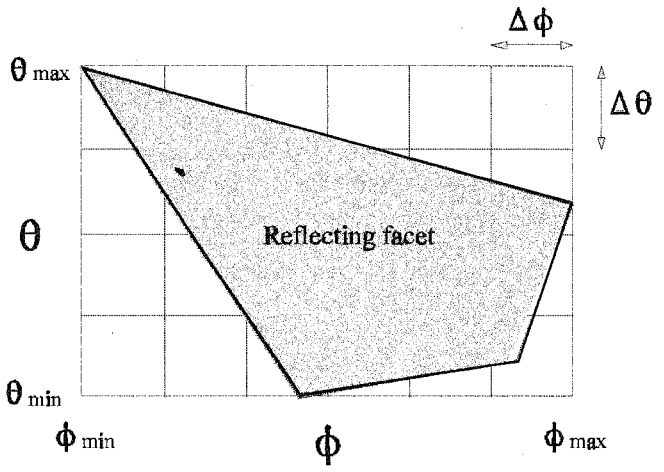

Figure 15. The AZB rectangle encloses in the θ_i, ϕ_i space, the reflecting facet as it is seen from source I. The facet is seen as a quadrangle with curved sides (the sides are drawn straight in the figure). The AZB rectangle is split into anxels.

DAZB matrix. The facets of each anxel are also arranged according to the distance from the source.

Given an observation point (O), its spherical coordinates (r_i, θ_i, ϕ_i) may not permit a reflection in the facet. Otherwise, it is checked to see if it lies in the reflection quadrangle. If it does not, there is not a reflection. Otherwise, the anxel of the observation point is found, and the facets located on the anxel are tested in order, following the same procedure as in the direct ray. With the above procedure, the possible hiding of the reflected ray is analyzed.

The analysis of the incident ray (from S to the reflection point) is done using the DAZB matrix of the direct field, taking the reflection point as the observation point.

5.4.3 Double-reflected-ray and higher-order-reflected ray case

Given a first-order image (I), only the facets located in the AZB rectangle can be involved in a double reflection. Then, for each of the above facets, the second-order image (I2) is determined. For each new source I2, the previous procedure is applied, that is, the AZB rectangle is obtained as for the first-order image (I).

For a given double-reflected ray, the possible hiding is analyzed as follows:

- For the incident ray (path transmitting-reflecting point 1), the DAZB matrix of the direct-field computation is used, considering the first reflection point as the observer.

- For the ray from reflecting point 1-reflecting point 2, the DAZB matrix of I is used, considering the second reflection point as the observation point.

- For the path reflecting point 2-observer, the DAZB matrix of I2 is used.

If high-order reflections are considered, the number of multiple images can be quite high. On the other hand, in high-order reflections, the reflecting space becomes very narrow (the margins of the AZB rectangle become very narrow), and the number of facets to store (and to test) becomes very low. As we will discuss in the comparison between the SVP and AZB techniques, in most second- and higher-order reflection cases the SVP technique will be preferable.

5.4.4 Vertex-diffracted rays

In this case, the application of the AZB algorithm is quite similar to the facet reflections. Now, instead of image points, there are vertex points.

5.4.5 Edge-diffracted rays

The application of the AZB algorithm to the edge-diffracted rays is, in part, different. Now, the sources are the points of the edges (infinite points). Moreover, each of these radiates in infinite directions, contained in the Keller cone. Therefore, an arrangement of the facets in the spherical coordinates θ, ϕ is not suitable. Instead of these, the coordinates β, α of the coordinate system fixed by the edge are used, in order to arrange the environmental facets as can be seen in Figure 16. β is the angle of the Keller cone at each edge point, so it varies along the edge. α is the angle between the diffracted ray and the first facet of the wedge.

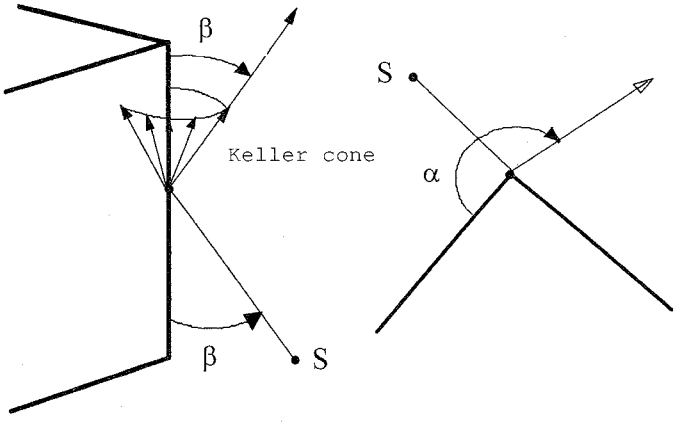

Figure 16. The definition of the β and α angular parameters for the AZB for edge diffraction.

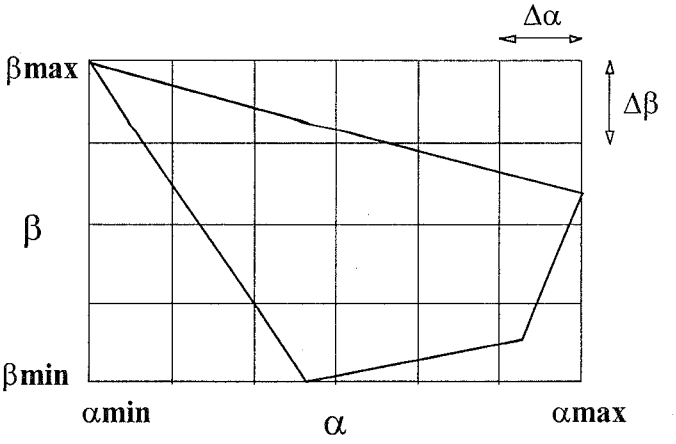

Figure 17. The definition of the AZB rectangle for edge diffraction.

Given a source S and an edge, all the diffracted rays can be represented as points in the so-called AZB rectangle of diffraction, as shown in Figure 17. This rectangle is a two-dimensional representation of the diffraction space. The maximum and minimum values of the edge coordinates (β_{max}, β_{min}, α_{max}, α_{min}) fix the margins of the rectangle. The rectangle is divided into anxels.

The facets of the environment are represented in the AZB rectangle as quadrangles. The vertices of the quadrangles are given by the edge coordinates of the facets' vertices.

The information about the AZB rectangles of diffraction depends on the geometry of the environment and on the source location. Therefore, it is independent of the observer point. This information is stored in the so-called DAZB matrix of diffraction.

Given an edge and an observation point, its edge coordinates (β_0, α_0) are calculated, and the point is located in the AZB rectangle. If it is outside the rectangle's margins, there is no diffraction at the edge. Otherwise, the anxel where the point lies is determined. Only the facets stored in the cell are considered in the testing of the diffracted-ray hiding. The test is made in an orderly way, that is, it begins with the facet closest to the edge, as was explained for the direct-ray case. Obviously, if a facet is farther from the edge than O, it is not tested.

If the diffracted ray is not hidden, the incident ray (source-diffraction point) is analyzed. The AZB matrix of the direct field is used for doing this task, taking the diffraction point as the observation point.

5.4.6 Reflected-diffracted rays

Only the edges located in the reflection space of the facets illuminated by the source are considered. These facets are obtained from the DAZB matrix of the direct field. Each one of these facets has its corresponding image of reflection. The DAZB matrices of diffraction are calculated as in the single-diffraction case, but now the sources are the images of reflection.

With this information, the shadow testing for reflected-diffracted rays is rapidly performed. If the observation point is not in the AZB rectangle of diffraction, there is no reflection-diffraction. Otherwise, the DAZB matrix of diffraction is used for the analysis of the diffraction point-observer line. The DAZB matrix of reflection is used for the analysis of the reflection point-diffraction point path, and the AZB matrix of the direct field is used in the S-reflection point line.

5.4.7 Diffracted-reflected rays

Only the edges stored in the DAZB matrix of the direct field can be involved in a diffraction-reflection. Also, only the facets stored in the DAZB matrices of single diffraction can take part in diffraction-reflection.

For each pair of edge-facets, the images of the source and edge in the reflecting facet are calculated, as shown in Figure 18. So, the problem is reduced to a single diffraction on the image facet, being the source the image of the transmitter I (this was calculated in the single-reflected-field computation). The DAZB matrix of diffraction of the image edge is calculated following a procedure similar to that of simple diffraction. The facets are

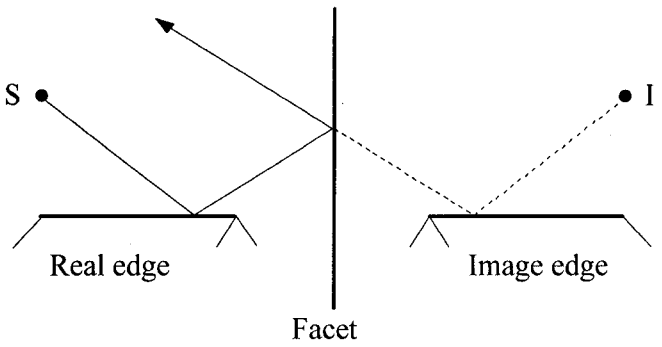

Figure 18. A diffraction-reflection is analyzed considering the images of the source and the edge.

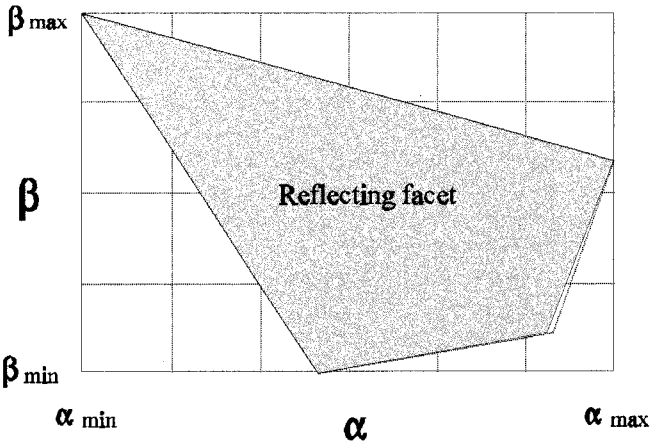

Figure 19. In an edge-diffraction problem, the reflecting facet is seen as a quadrangle. The AZB rectangle of the image edge encloses the quadrangle. This quadrangle has, in general, a curved side (in the figure, the sides are drawn straight).

located in the AZB rectangle. With this information, for any observation point, the ray tracing is rapidly solved: Only the observation points located inside the quadrangle of the reflecting facet are involved in a diffraction-reflection (see Figure 19).

The DAZB matrix of the image edge is used for the analysis of the reflection point-observer path. The AZB matrix of the real edge is used for the analysis of the path between the diffraction point and the reflection point. Finally, the line S-diffraction point is analyzed, using the DAZB matrix of the direct field.

5.4.8 Application to multiple interactions between edges and facets

The shadow testing of multiple interactions involving reflections and diffraction can be solved by combining the above procedures. If the number of diffraction events and/or reflections is high, the number of DAZB matrices grows, and more memory is necessary. On the other hand, in high-order effects, the margins of the AZB rectangles become very narrow, so the number of facets to be stored (and to be tested) becomes very low.

5.5 Comparison between the SVP and the AZB techniques

Comparing the shadow testing of the path SO, using the mesh by voxels of the SVP technique (Figure 9), with the mesh by anx-

els of the AZB technique (Figure 11), it can be concluded that the AZB technique checks a smaller number of facets. In particular, the SVP technique can be required to check all the facets of all the voxels that the SO path crosses. That is because the facets are randomly stored in the SVP matrix, without any order regarding their positions relative to the SO path. However, when the AZB is used, the facets are stored in accordance with their proximity to the source–thanks to the Painter's algorithm–and the probability of determining a shadow or a visibility observation point, checking only one or two facets, is quit high. So, in principle, the AZB appears to be more efficient for the shadow testing of a given SO path.

However, the effort required to form the DAZB and SVP matrices must also be analyzed. The SVP technique only requires forming one matrix that, on the other hand, only depends on the scene. The SVP matrix is independent of the source position, whatever the nature of the source may be: the original transmitter, the reflection-images, the diffraction points, etc. To the contrary, the DAZB matrices depend on the scene and also on the source position to be considered (original transmitter, images, etc.). In a typical urban scene, the number of DAZB matrices can be very large.

From the above discussion, it can be concluded that the SVP and the AZB techniques have their pros and cons. The AZB technique is superior when a large number of observation points are to be checked, as occurs for the direct-ray case, diffracted-ray cases, and for the reflection of facets with a large AZB rectangle. But when the number of points to be checked is small–for instance, in a double-reflection with a small rectangle for the second facet– the effort required to form the DAZB matrix is not recovered in the shadow testing, and in these cases, the SVP is preferable.

In conclusion, it can be stated that it would be best to combine both techniques: the AZB for sources covering a large number of observation points, and the SVP for the rest of the sources.

6. Validation

In order to check and validate some of the ray-tracing approaches presented, a *FORTRAN* code, called *FASPRO*, has been implemented. The *FASPRO* code mainly uses AZB. The code works with three-dimensional structures, and is based on a UTD/GTD formulation similar to this one described in [15]. All the edges (horizontal or vertical) of the scene are considered in the diffraction computation. Double diffraction has not been included, because its contribution to the field level has been found to be negligible in all the situations considered.

The urban scenario of Figure 1 has been chosen as the first case for the validation. This scenario corresponds to the commercial center of Madrid. Figure 20 presents a map of this urban scene. The area of the map has a size of 1,050 × 1,450 square meters. The geometrical data were provided by a company specializing in cartographic-data acquisition, which carried out specific topographical flights. A three-dimensional geometric model (in *DXF* format) was provided, with an error which was assumed to be less than 1 m. In the analysis, all the scenario materials (ground and buildings) were assumed to be made of concrete.

The transmitting antenna is located at a height of 7 m above the ground level; it radiates a power of 14 dBm, and its frequency is 945 MHz. The radiation pattern of this antenna is described by its E- and H-plane cuts. Figure 21 pictures the E-plane cut of the transmitting antenna (the H-plane cut is very similar).

The measurements have been carried out along the paths indicated in Figure 20. Three paths are considered. One path is completely located in the same street–the line-of-sight (LOS) street–as the transmitting antenna. This path has a length of approximately 1000 m, and it is bounded in Figure 20 by the numbers 1 and 999. A second path, of length 50 m, is in a street perpendicular to the antenna street, and it is bounded by numbers 1 and 50. The third path, bounded by the numbers 1 and 200, is along a street parallel to the LOS street, as can be seen in Figure 20, and has a length of 200 m. In the three cases, several samples per wavelength of path were taken. A GPS system was used to accurately record the position for each sample in the measurements. Therefore, a quite accurate digital representation of the path in the measurements was obtained. This representation was also considered in the computations.

The receiving antenna is assumed to be a short dipole, at a height of 1.5 m above the ground. In order to avoid errors in the comparison between measurements and computations due to the fast fading, an average of the field was taken. For both measure-

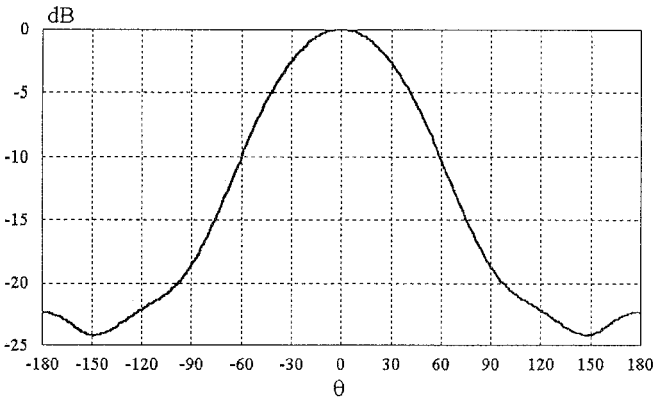

Figure 21. An E-plane cut of the transmitting-antenna radiation pattern.

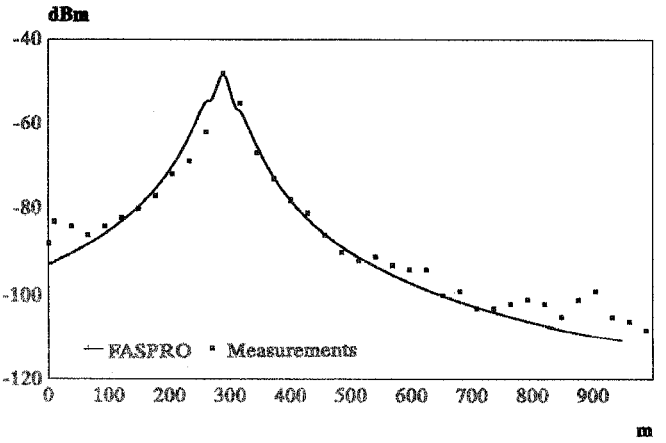

Figure 22. A comparison between computations and measurements. Only the direct field and the ground-reflected fields have been considered in the computations. This means that the computed values are identical to those of the "two-ray model." We can see that the predictions in the LOS street with this model are not bad. The discrepancies between measurements and computations near the maximum of the field level could be due to errors in the antenna-axis orientation and/or in the radiation pattern considered.

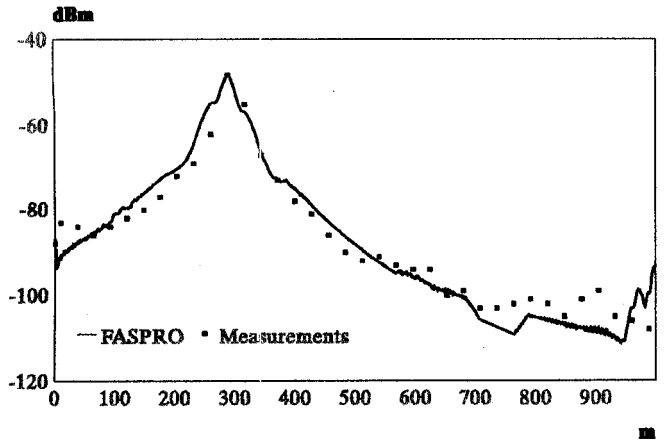

Figure 23. The same case as in Figure 22, but now considering all the simple effects (direct ray, reflected rays, and diffracted rays). Second-order effects (reflection-diffraction, diffraction-reflection, and double reflection), with one of the effects being a reflection in the ground, have also been taken into account. The correction that the new coupling mechanisms introduce is quite small, and located far away from the maximum level. The field level tends to increase in zones far away from the transmitting antenna, especially in the areas covered by the reflection of the large buildings in the street sides.

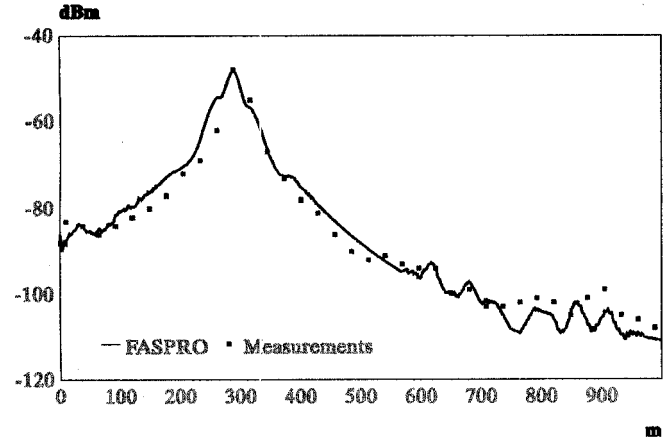

Figure 24. The same case as in Figure 22, but now considering all the effects of Figure 23 plus the following double effects: double-reflected rays, diffracted-reflected rays, and reflected-diffracted rays. Triple effects are also included, when one of the effects in the triad is a reflection in the ground. No double diffraction is included, because its field level has been found to be negligible in comparison with the rest of the effects. The correction that the new coupling mechanism introduces is quite small, except in the areas far away from the transmitter, where the measured fields are about 50 dB bellow the maximum. In these areas, the double or triple effects contribute to increasing the computed values to a level very close to the measurements.

ments and computations, the field at each point is averaged by considering the field value at the point and at the 11 nearest points.

The comparisons between measurements and computations for the LOS street are shown in Figures 22-24, considering different numbers of coupling mechanisms. We can note that the "two-ray model," considered in Fig 22 (only direct rays and ground-reflected rays), provides, in general, good results. The exception is in zones far away the transmitter, where the field level is low, and where other ray mechanisms become important. In these zones, the correction due to the rest of the simple effects (Figure 23) and double effects (Figure 24) gives reasonably good results.

The results along the second path, in the perpendicular street, are presented in Figures 25-26. Now, the situation for the computations is considerably more difficult than for the LOS street. There are no direct rays or even simply reflected rays reaching the path. Therefore, the first results we present, Figure 25, include diffracted rays. Examining this figure, we find that computations are always below measurements, with differences of about 20 dB. It appears evident than more ray effects should be considered to improve the accuracy of the predictions. Figure 26 shows the results obtained considering second- and some of the third-order effects. Now the agreement between computations and measurements looks very good.

The third path, in the parallel street, represents a very demanding case for the calculation, in microcell environments. The path is in a zone with a severe shadow relative to the transmitter.

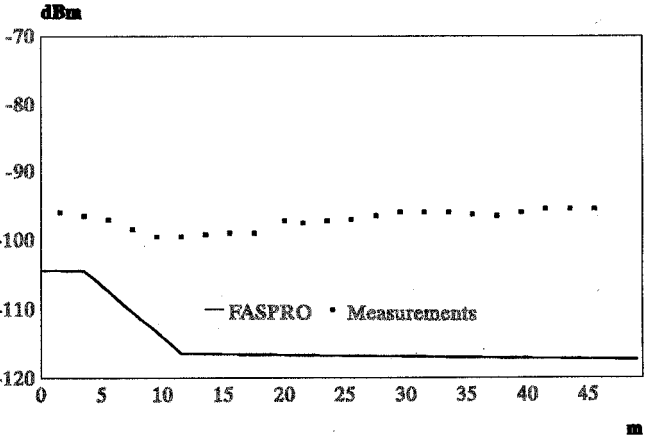

Figure 25. A comparison between measurements and computed values along the perpendicular street, considering the simple and double effects defined in Figure 23. A large difference between both kinds of results appears evident.

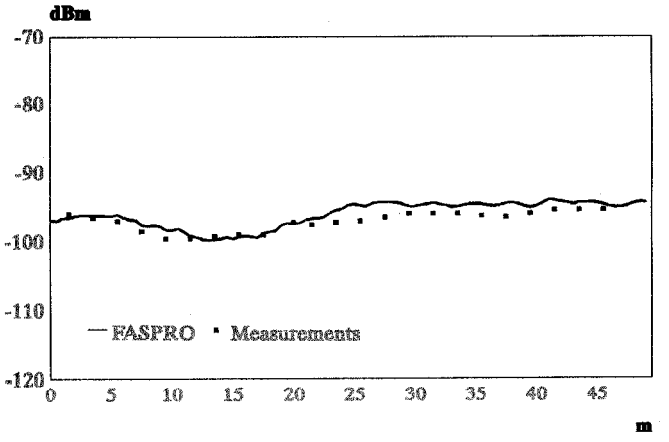

Figure 26. A comparison between computations along the path in the perpendicular street. Now all the simple, double, and triple effects, defined in Figure 24, have been considered. The accuracy of the numerical prediction appears to be quite fine.

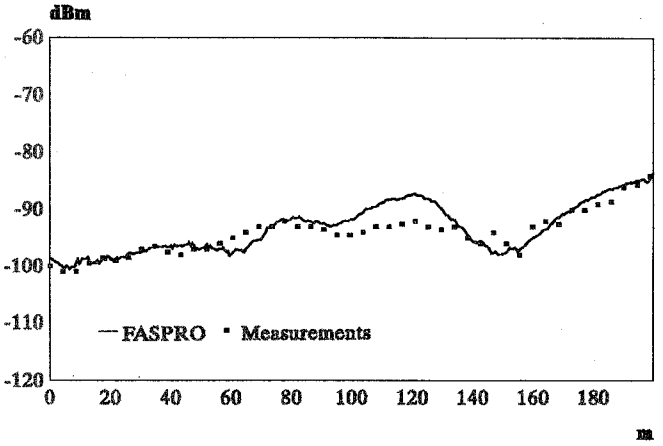

Figure 27. The computed and measured field level along the path in the parallel street. The computations included all the simple, double, and triple effects considered in Figure 24. The average value of the field level is approximately of the same order as that in Figure 26.

Surprisingly, the field level is not too much lower than in the case of the perpendicular street. Now, again and as shown in Figure 27, the predicted values with second- and third-order effects are good enough, at least for applications in cellular planning.

The urban scenario of Figure 1 can be representative of a "large skyscraper" environment. *FASPRO* has been also checked considering more "moderate" urban environments, such as those presented in reference [7] for the cases of Tokyo and Manhattan. Good agreement between computations and measurements were also obtained for these cases. For instance, Figures 28 and 29 show results from *FASPRO* considering simple and second-order effects for the path lines CAD and EBF, respectively, of the Tokyo case in reference [7]. In both figures, 1000 points on the horizontal axis are equivalent to 700 m. The field at each point was computed considering the average of the GTD/UTD values in the neighboring 10 points. It can be noted that the *FASPRO* results fit very well to the measurements, considering the error margins indicated in Figures 4 and 5 of reference [7]. Similar agreement between computed and measured values has been obtained for the Manhattan case.

Regarding the accuracy of the models and of the FASFRO code, we can distinguish two kinds of errors: a) in the input data, and b) due to the computer UTD and ray-tracing approach. Among the input-data errors, we can mention the inaccuracies in the topographical and morphological data of the urban scene and in the antenna input data (radiation pattern, position, and orientation). From the authors' experience, the impact of the errors of the antenna data can often times be more important than the error in the rest of the input data.

The UTD/GTD model introduces several errors, among them the following: a) the error inherent in UTD, due to the finite size of the obstacles; b) the approximations in the treatment of reflection and diffraction in dielectric material; c) the approach of considering the surfaces of the buildings and the ground to be perfectly flat planes; and d) the assumption that the surfaces are smooth and do not give diffuse reflections. Errors in the ray-tracing algorithm and in its code implementation also can appear. One can never be sure that the code and the ray-tracing algorithms run as they were planned. Fortunately, most times these latter errors are so evident that they are easy to identify and, consequently, to correct.

Summarizing the error evaluation of our approach and code, we can say that the average error is in a band between 3 to 6 dB, and seldom is the error greater than 10 dB.

The CPU time using *FASPRO* for the cases of Figures 22-27 on a Pentium computer (120 MHz, 32 MB of RAM) has been a few minutes per case. This is a very short time, taking into account that the total number of facets in the scene is about 700, and the number of observation points is several hundred. For the case of Figure 4, the field has been computed at 62,500 observation points, considering double effects and some of the triple effects (those with one effect in the triad being a ground reflection). The CPU time is about 45 minutes. For most applications, the number of facets in the scene can be about 300, and the number of observation points about 10,000. In this last case, the CPU time is about five minutes for the simple, double, and triple effects considered in Figures 4 or 24.

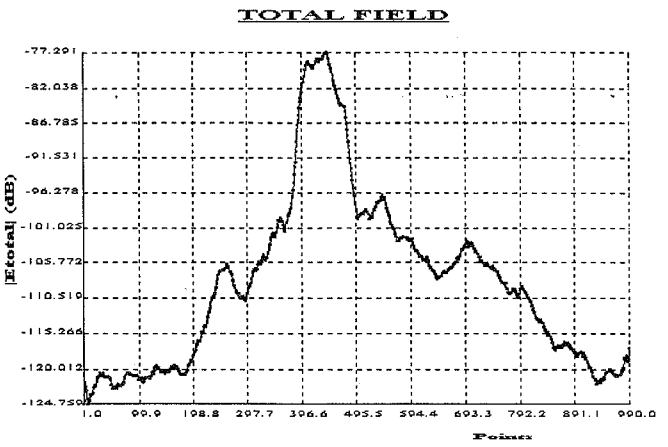

Figure 28. *FASPRO* results for the path loss along the CAD line, considering simple and double effects, except double-diffraction, for the Tokyo case in reference [7].

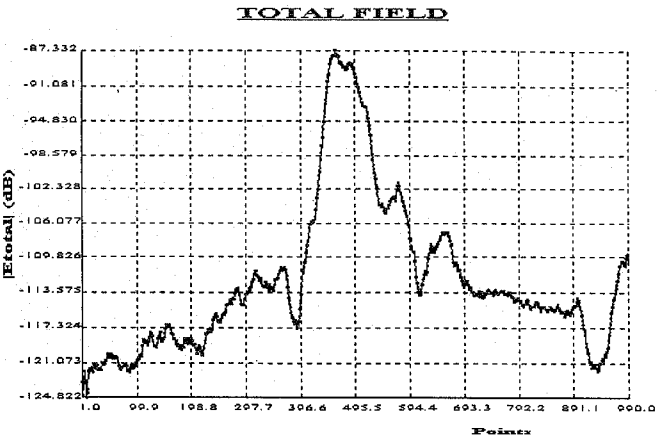

Figure 29. FASPRO results for the path loss along EBF line, considering simple and double effects, except double-diffraction, for the Tokyo case in reference [7].

7. Conclusions

It has been shown that modern ray-tracing algorithms, in combination with the UTD/GTD technique, can provide a method for the planning of cellular communications. The CPU time and accuracy appear to be appropriate for this purpose.

Further details about the algorithms or about he code presented in the paper can be obtained by directing inquires to Felipe Catedra *(felipe@gsr.unican.es)*.

8. References

1. D. Parsons, *The Mobile Radio Propagation Channel*, London, Pentech Press Limited, 1992.

2. T. S. Rappaport, S. Y. Seidel, K. R. Scaubach, "Site-Specific Propagation for PCS System Design," in M. J. Feuerstein and T .S. Rappaport (eds.), *Wireless Personal Communications*, Boston, Kluwer Academic Publishers, 1993, pp. 281-315.

3. S. Y. Seidel and T. S. Rappaport, "Site-Specific Propagation Prediction for Wireless In-Building Personal Communication System Design," *IEEE Transactions on Vehicular Technology*, **VT-43**, 4, November 1994, pp. 879-891.

4. K. R. Schaubach and N. J. Davis, "Microcellular Radio-Channel Propagation Prediction," *IEEE Antennas and Propagation Magazine*, **36**, 4, August 1994, pp. 25-34.

5. J. W. McKown and R. L. Hamilton, "Ray Tracing as a Design Tool for Radio Networks," *IEEE Network Magazine*, November 1991, pp. 27-30.

6. M. C. Lawton and J. P. McGeehan, "The Application of a Deterministic Ray Launching Algorithm for the Prediction of Radio Channel Characteristics in Small-Cell Environments," *IEEE Transactions on Vehicular Technology*, **VT-43**, 4, November 1994, pp. 955-969.

7. S. Y. Tan and H. S. Tan, "A Microcellular Communications Propagation Model Based on the Uniform Theory of Diffraction and Multiple Image Theory," *IEEE Transactions on Antennas and Propagation*, **AP-44**, 10, October 1996, pp. 1317-1326.

8. A. S. Glassner (ed.), *An Introduction to Ray Tracing*, San Diego, Academic Press, 1989.

9. J. D. Foley, A. van Dam, S. K. Feiner, and J. F. Hughes, *Computer Graphics: Principles and Practice, Second Edition*, New York, Addison-Wesley, 1995.

10. R. C. Gonzalez and R. E. Woods, *Digital Image Processing*, New York, Addison-Wesley, 1993.

11. H. S. Rubin and T. Whitted, "Three-Dimensional Representation for Fast Rendering of Complex Scenes," *Computer Graphics* (Proceedings of SIGGRAPH 80), 1980, pp. 110-116.

12. M. Kaplan, "Space-Tracing: A Constant Time Ray-Tracer," course notes from the tutorial "State of the Art in Image Synthesis," SIGGRAPH 85, 1985.

13. E. A. Hines and D. P. Greenberg, "The Light Buffer: A Shadow-Testing Accelerator," *IEEE Computer Graphics & Animation*, September 1986, pp. 6-16.

14. M. E. Newell, R. G. Newell, and T. L. Sancha, "A Solution to the Hidden Surface Problem," *Proceedings of the ACM National Conference 1972*, pp. 443-450.

15.] A. G. Kanatas, I. D. Kountouris, G. B. Kostaras, and P. Constantinou, "A UTD Propagation Model in Urban Microcellular Environments," *IEEE Transactions on Vehicular Technology*, **VT-46**, February 1997, pp. 185-193.

Introducing Feature Article Authors

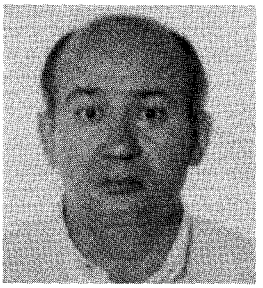

Manuel F. Catedra received his MS and PhD degrees in Telecommunications Engineering from the Polytechnic University of Madrid (UPM) in 1977 and 1982, respectively. From 1976 to 1989, he was with the Radiocommunication and Signal Processing Department of the UPM, teaching and doing research. He became a full Professor at Cantabria University in 1989.

He has worked in about 25 research projects, solving problems of electromagnetic compatibility in radio and telecommunication equipment, antennas, microwave components and radar cross section, signal processing, and mobile communications. He has developed and applied CAD tools for radio equipment systems such as warships, aircraft, helicopters, satellites, and antenna-array processors. The main contractors for this work have been Spanish or European institutions, such as CASA, ALCATEL, BAZAN, TELEFONICA, the Spanish Defence Department, SAAB, and MATRA. He has directed about twelve PhD dissertations, has published about 30 papers, two books, about 10 chapters in books, and has presented around one hundred presentations in international symposia.

Jesús Pérez was born in Santander, Spain, in 1969. He received the MS degree in Physics from the University of Cantabria, Spain, in 1989, and the PhD in Physics from the University of Cantabria, in 1994. In 1989, he was with the Radiocommunication and Signal Processing Department of the Polytechnic University of Madrid as a research assistant. From 1990 to 1992, he was with the

Electronics Department of the University of Cantabria as a research assistant. In 1993, he became an Assistant Professor in the Electronics Department of the University of Cantabria. He has participated in several research projects with Spanish and European companies, related to RCS computation, analysis of on-board antennas, radio propagation in mobile communications, etc. He is the author of six papers and of more than 20 conference contributions at international symposia. His research interests include high-frequency methods in electromagnetic radiation and scattering, and geometrical modeling in electromagnetic and mobile communications.

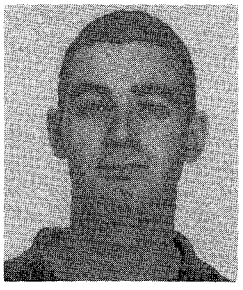

Francisco Saez de Adana was born in Santander, Spain, in 1972. He received the BS and MS degrees in Telecommunications Engineering from the Cantabria University in 1993 and 1996, respectively.

He has been with the Communications Engineering Department of the Cantabria University since 1995, where is pursuing the PhD degree. His research interests are in areas of electromagnetic radiation, on-board antenna analysis, and mobile communications.

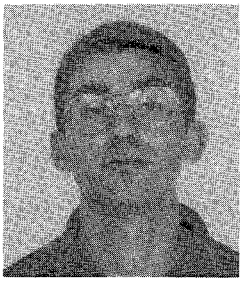

Oscar Gutiérrez Blanco was born in Torrelavega, Spain, in 1970. He received the BS and MS degrees in Telecommunications Engineering from the University of Cantabria, Spain, in 1993 and 1996, respectively.

He has been with the Communications Engineering Department of the University of Cantabria since 1995. His research interests are in on-board antenna analysis, and propagation modeling for mobile communications.

Editor's Comments *Continued from page 6*

Publish! I attended the IEEE Press Board meeting in La Jolla recently. I was impressed. This is not the same organization it was two years ago. It has hired staff with significant experience in the technical-publishing field, including editing, acquisitions and new titles, and marketing. The Press now has joint marketing arrangements with Oxford University Press, and is creating liaisons with other very important strategic partners. The titles recently published and in the works are very solid from both the technical and the market perspectives, and they are selling *very* well. In particular, AP-S can be extremely proud of what has been accomplished by the IEEE/OUP Electromagnetic Wave Series, under the leadership of Series Editor Don Dudley. Bob Mailloux has also done an excellent job as AP-S IEEE Press Liaison Committee Chair. If you have any thought of publishing a book, give the IEEE Press careful consideration. I think you'll be glad you did.

Getting involved. We live in interesting times. All signs in the US point toward a demand for engineers that is higher than we've seen for perhaps more than 20 years. At the same time, I've seen studies indicating that some US employers are hiring fewer than 5% of qualified applicants. It seems that many employers are seeking those with less experience, because they will work for lower salaries. There also is currently a great debate in the US over whether or not to raise the limits on how many technically qualified immigrants can come to work here. Again, industry is pushing for this as a way to solve the "problem of the shortage of qualified engineers." Most of the independent studies I've seen point to the existence of such a "shortage" as being *very* questionable, at the least. The conclusions of most such studies are that if there is any shortage, it is a perceived (on the part of industry) shortage of *low-cost* engineering talent. When you couple this with statistics showing only very modest recent increases in average engineering salaries, it is not a very pretty picture. If you are in the US, you might want to get involved in contacting your government representatives regarding this. Information can be found (although with more difficulty than I think should be necessary!) on the IEEE-USA's Web page, at http://www.ieee.org/usab. A specific item related to this controversy is located at the following URL: http://www.ieee.org/usab/DOCUMENTS/FORUM/LIBRARY/legisrep.html#head1

There are some indications that this may be less of a trend in our specific field, and that experience is being valued in at least some cases. I hope that your work environment values you–just as we value you as a reader.

Roll